Supporting Information

Thin film TiO_2/TiN bifunctional interface enables integration of Ni_5P_4 electro-catalyst with $GaInP_2$/GaAs III-V tandem photoabsorber for stable solar-driven water splitting

Shinjae Hwang,[1,6] Hengfei Gu,[1,6] James L. Young,[2] Myles A. Steiner,[2] Anders B. Laursen,[1] Ryan A. Crichton,[1] Yao-Wen Yeh,[3] Philip E. Batson,[3] Leonard C. Feldman,[3,4] Mengjun Li,[1] Keenan Wyatt,[2] Ahmad Safari,[4] Todd G. Deutsch,[2] Eric Garfunkel*[1] and G. Charles Dismukes*[1, 5]

[1]Department of Chemistry and Chemical Biology, Rutgers, The State University of New Jersey, Piscataway, New Jersey 08854, United States.

[2]National Renewable Energy Laboratory, 15013 Denver West Parkway, Golden, Colorado 80401, United States.

[3]Department of Physics and Astronomy, Rutgers, The State University of New Jersey, Piscataway, New Jersey 08854, United States.

[4]Department of Materials Science & Engineering, Rutgers, The State University of New Jersey, Piscataway, New Jersey 08854, United States.

[5]Waksman Institute, Rutgers, The State University of New Jersey, Piscataway, New Jersey 08854, United States.

[6]These authors contributed equally: Shinjae Hwang, Hengfei Gu.

*Corresponding authors. E-mail: egarf@chem.rutgers.edu; dismukes@chem.rutgers.edu

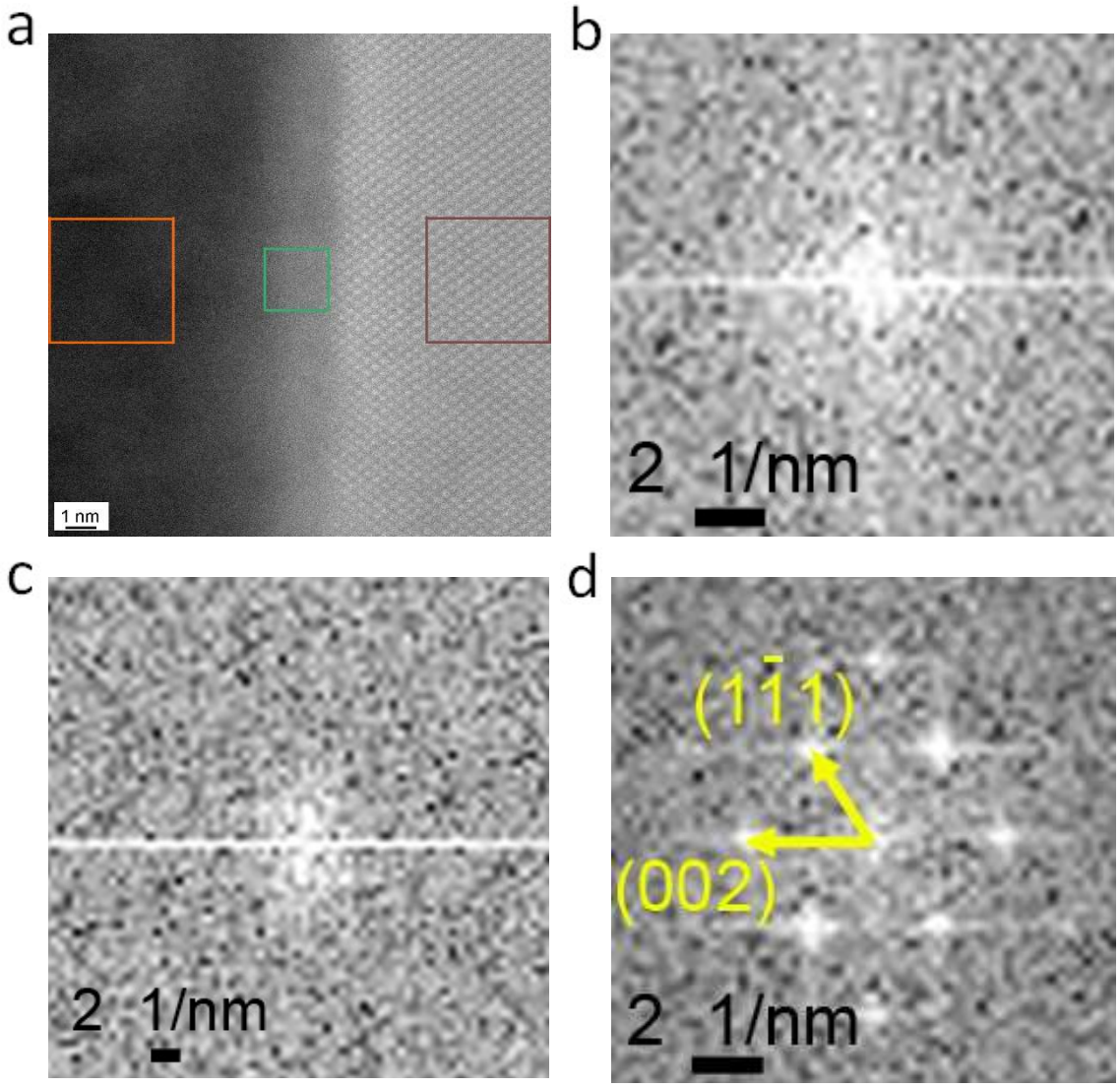

Figure S1 Fast Fourier transformation (FFT) analysis of the HAADF image of the TiO_2/TiN/$GaInP_2$ interface. a, HAADF image of the TiO_2/TiN/$GaInP_2$ interface. **b-c**, FFT patterns corresponding to the regions boxed by orange, green and brown lines, respectively, corresponding to the TiO_2, TiN and $GaInP_2$ layers.

Table S1 Compositional analysis of the TiO_2 and Ni_5P_4 films

Sample	Ti (at. %)	O (at. %)	Ni (at. %)	P (at.%)
TiO_2/III-V tandem	36.1 ± 0.2	63.9 ± 0.2	N/A	N/A
TiO_2/TiN/III-V tandem	35.9 ± 0.6	64.1 ± 0.6	N/A	N/A
Ni_5P_4/TiO_2/III-V tandem	N/A	N/A	15.6 ± 0.2	84.4 ± 0.2
Ni_5P_4/TiO_2/TiN/III-V tandem	N/A	N/A	11.1 ± 0.7	89.9 ± 0.7

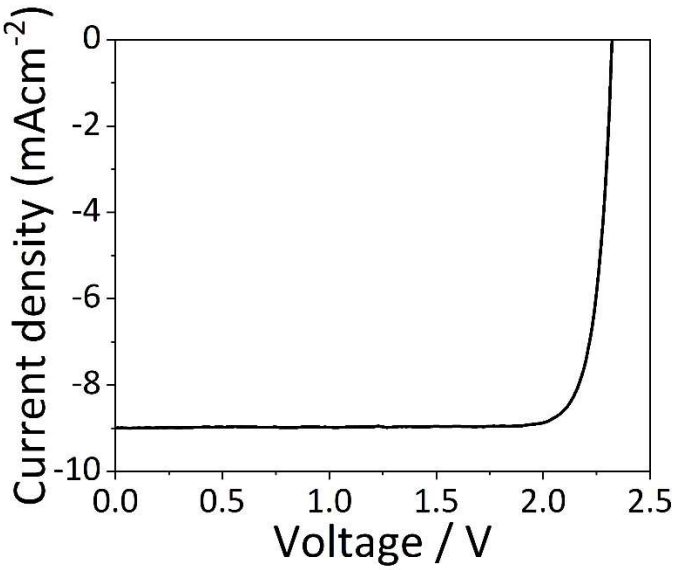

Figure S2 J-V curves of $GaInP_2$/GaAs III-V tandem solar cell under AM 1.5G simulated solar illumination.

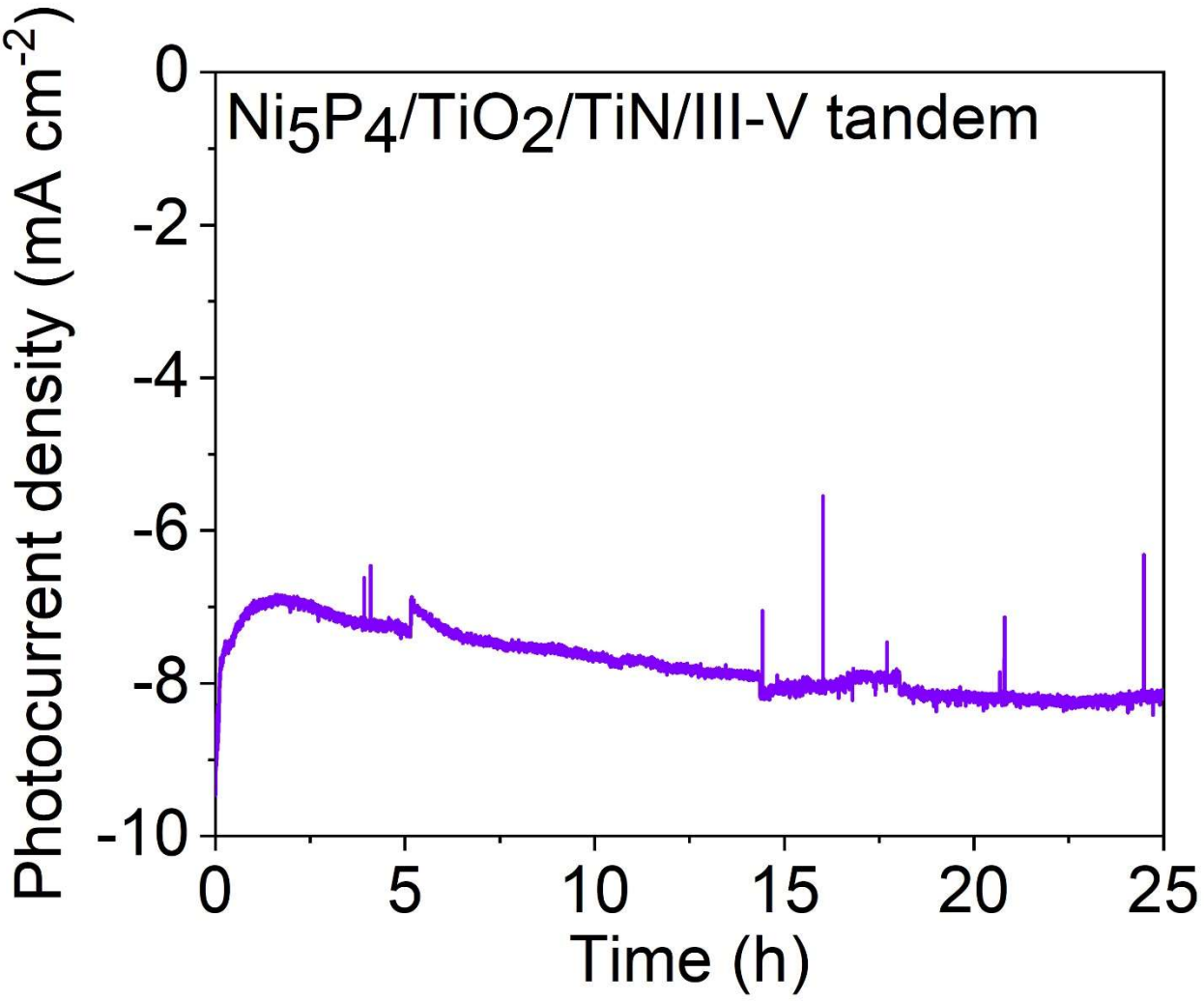

Figure S3 CA curve as a function of time of the Ni_5P_4/TiO_2/TiN/III-V photocathode measured in pH7 sodium phosphate buffer solution under one-sun illumination in a two-electrode configuration.

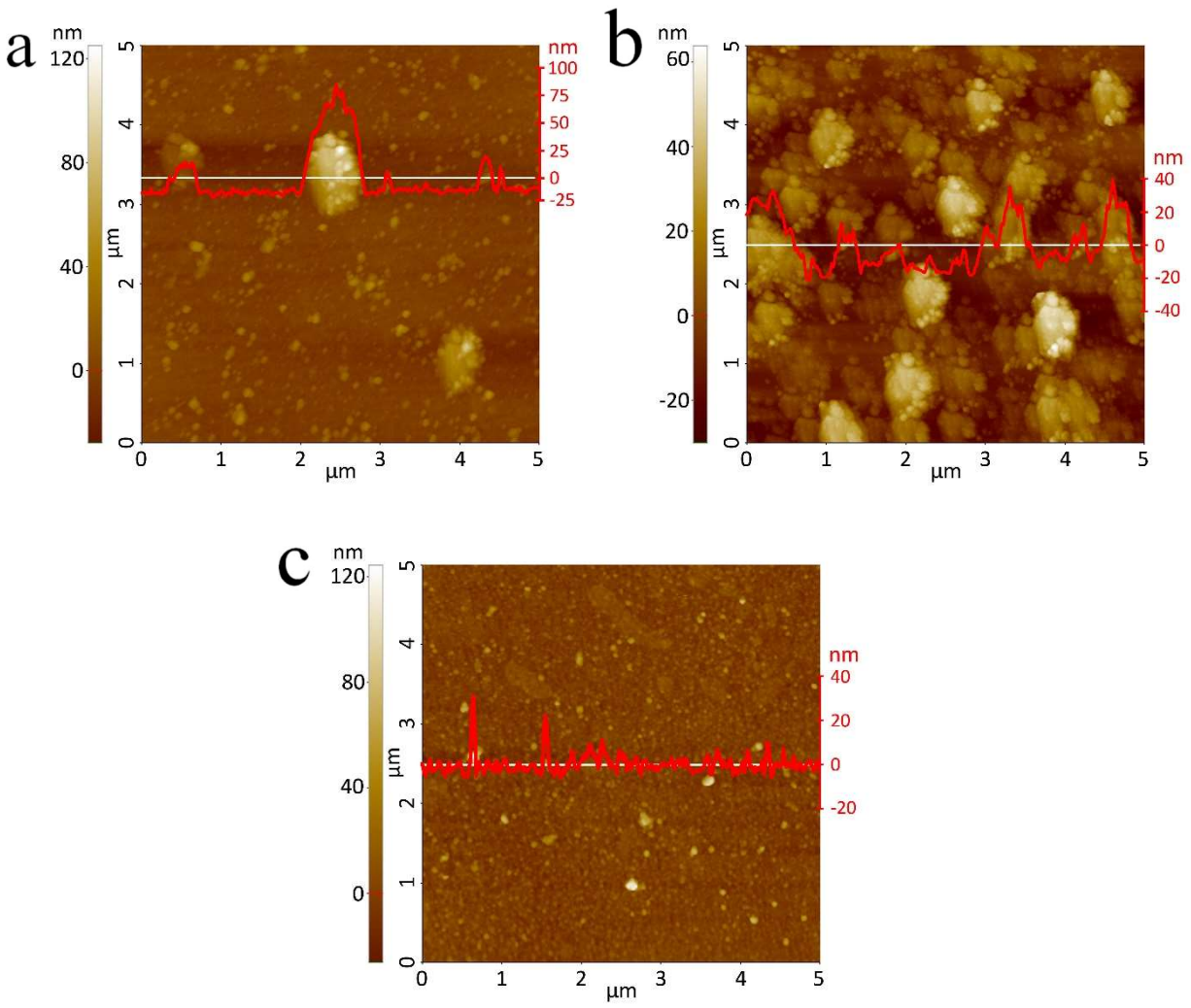

Figure S4 AFM post-analysis of the surfaces of the $Ni_5P_4/TiO_2/TiN/GaInP_2/GaAs$ III-V tandem photocathodes. **a-b** and **c**, AFM images of the photocathode surface after the CA durability analysis for ~ 5 h and ~ 25 h (at and after the photocurrent current crest in **Figure 8a**), respectively.

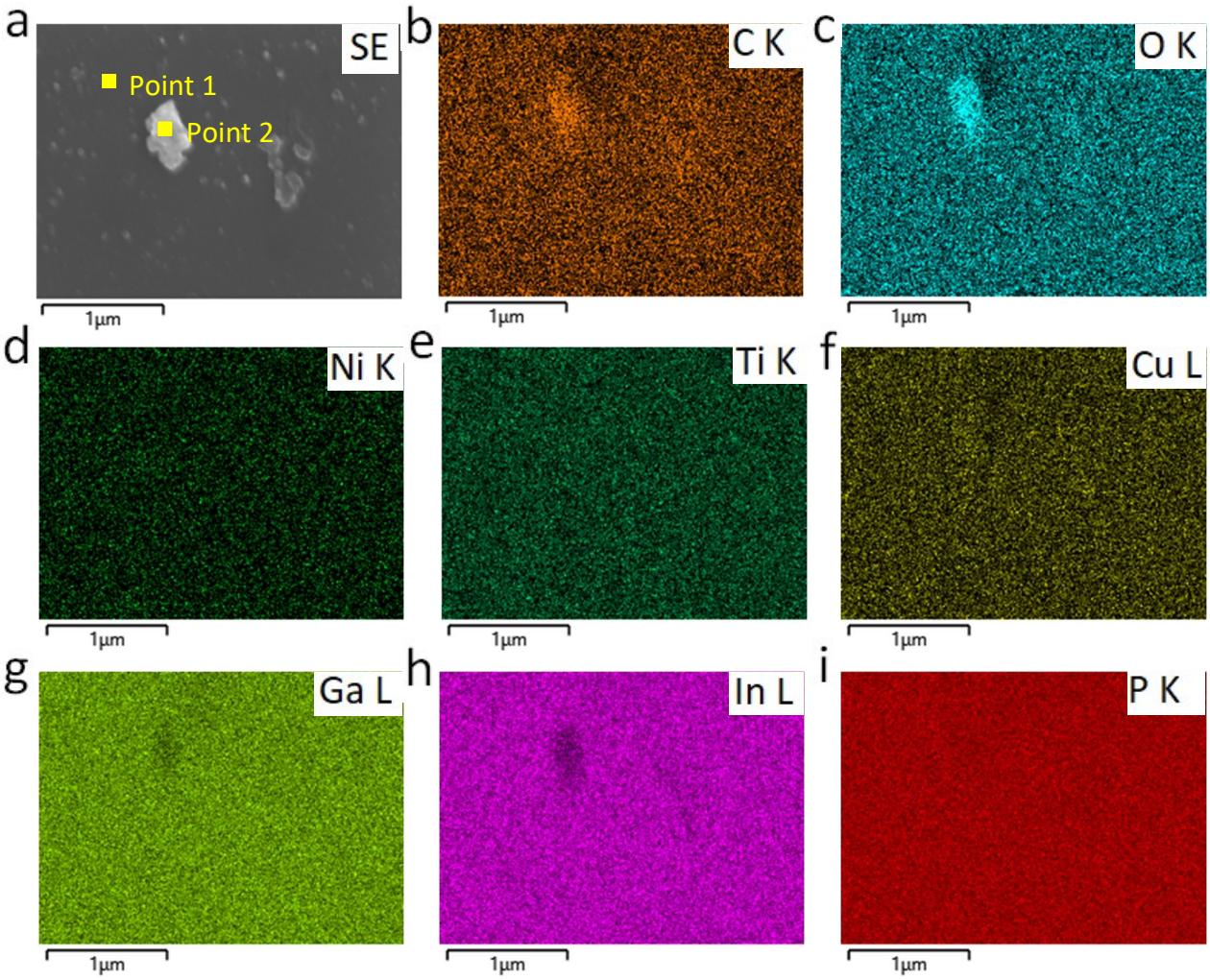

Figure S5 Energy-dispersive X-ray (EDX) spectroscopy elemental mapping of the surface of $Ni_5P_4/TiO_2/TiN/GaInP_2/GaAs$ III-V tandem photocathode after ~ 5 h for continuous unassisted water splitting in a two-electrode configuration coupling with an IrO_2-coated carbon paper anode in 0.5 M sodium phosphate (pH7) under simulated 1 sun illumination.

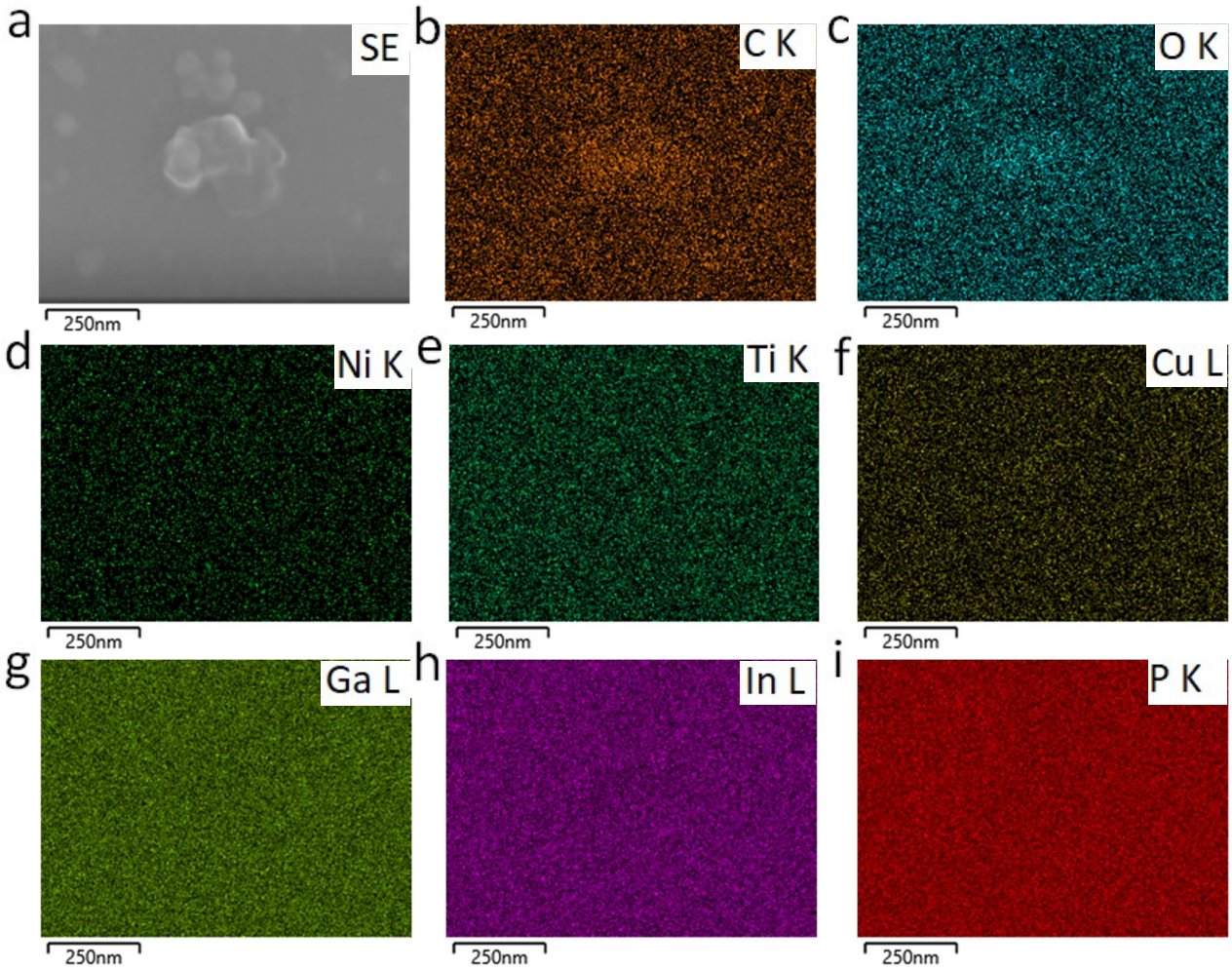

Figure S6 EDX spectroscopy elemental mapping of the surface of $Ni_5P_4/TiO_2/TiN/GaInP_2/GaAs$ III-V tandem photocathode after ~ 5 h for continuous unassisted water splitting in a two-electrode configuration coupling with an IrO_2-coated carbon paper anode in 0.5 M sodium phosphate (pH7) under simulated 1 sun illumination.

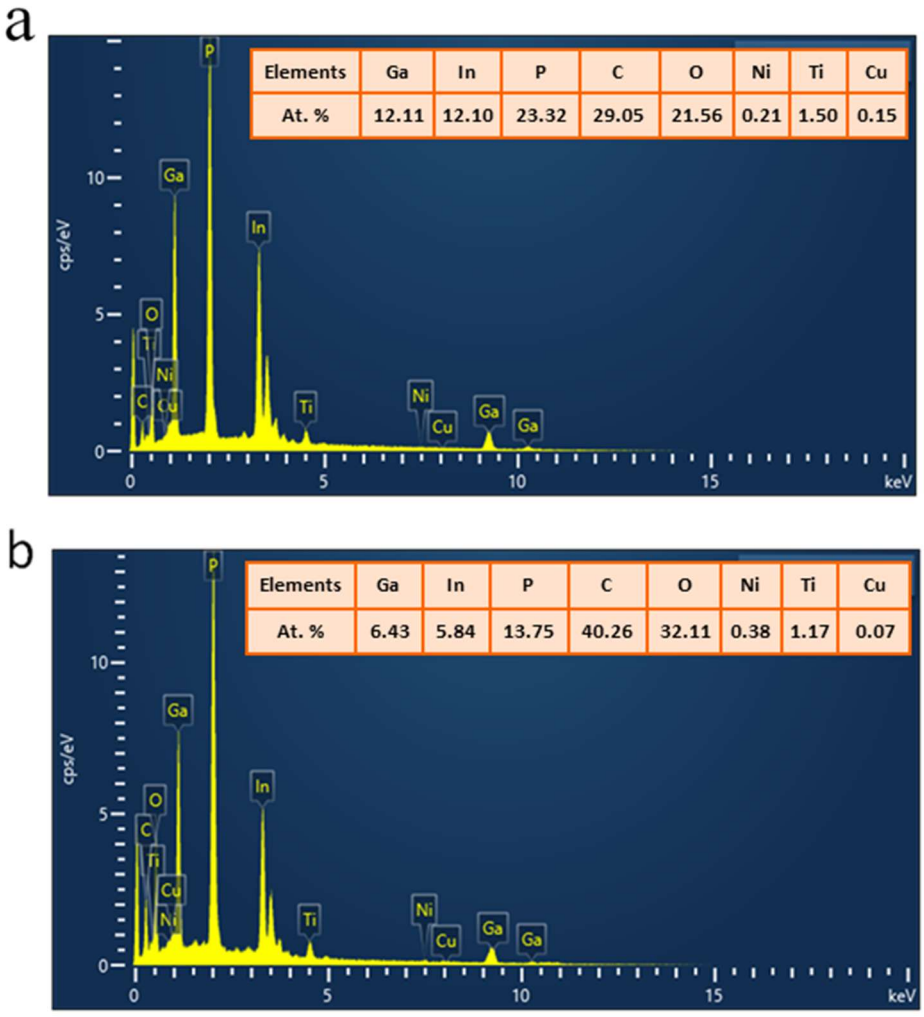

Figure S7 a-b, EDX spectra of Point 1 and 2 in **Figure S5a**.

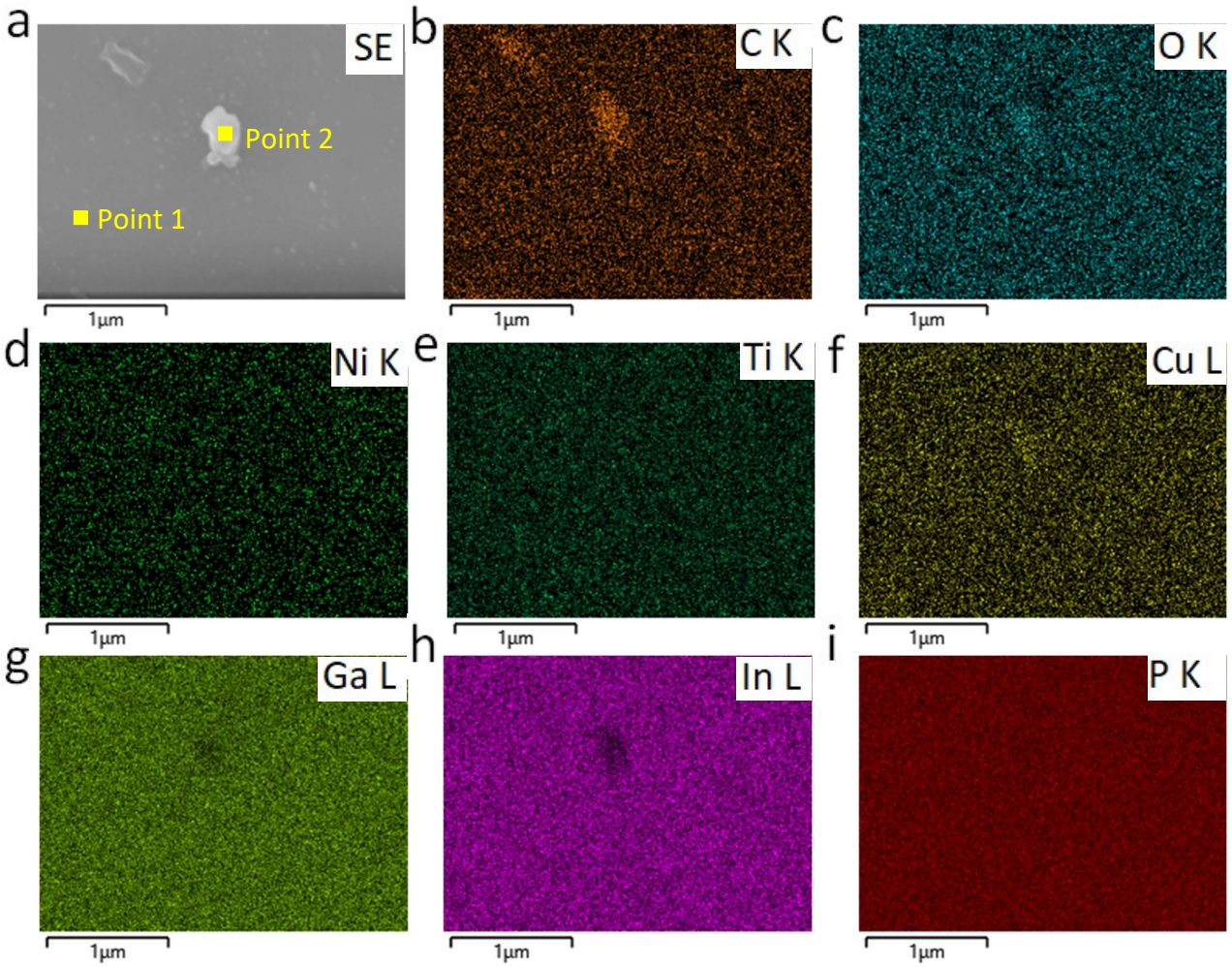

Figure S8 EDX spectroscopy elemental mapping of the surface of $Ni_5P_4/TiO_2/TiN/GaInP_2/GaAs$ III-V tandem photocathode after ~ 25 h for continuous unassisted water splitting in a two-electrode configuration coupling with an IrO_2-coated carbon paper anode in 0.5 M sodium phosphate (pH7) under simulated 1 sun illumination.

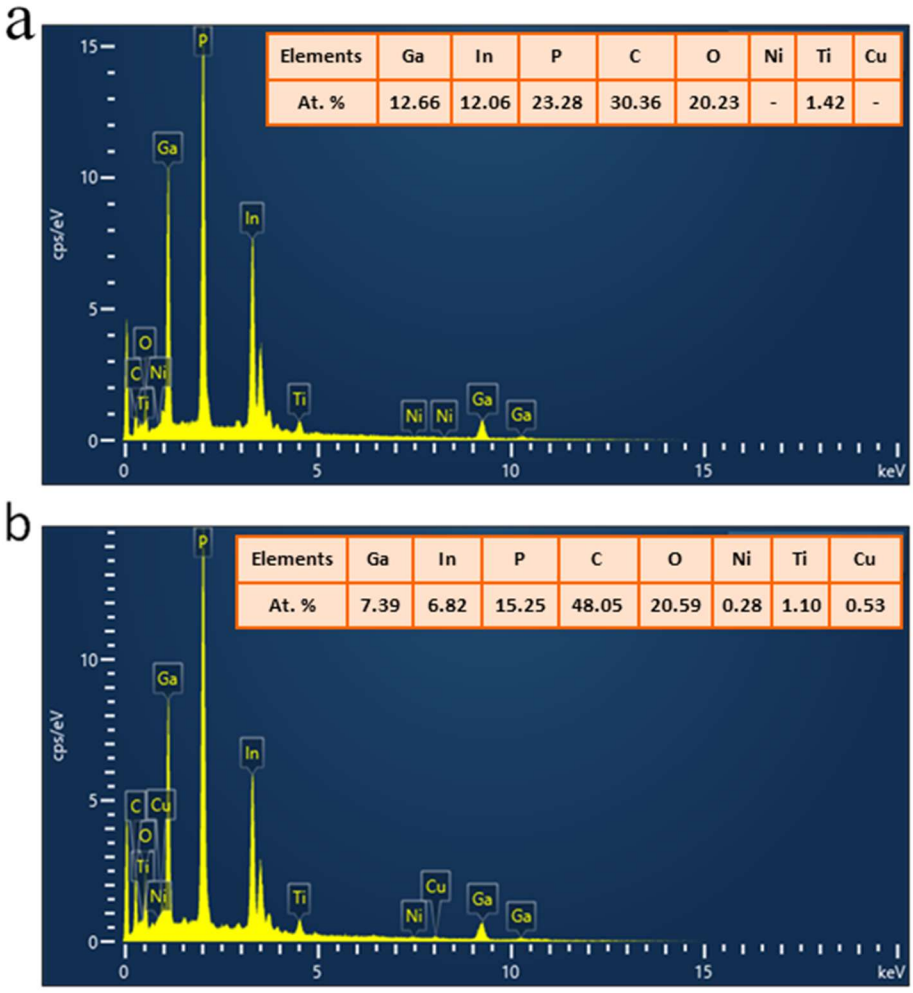

Figure S9 a-b, EDX spectra of Point 1 and 2 in **Figure S8a**.

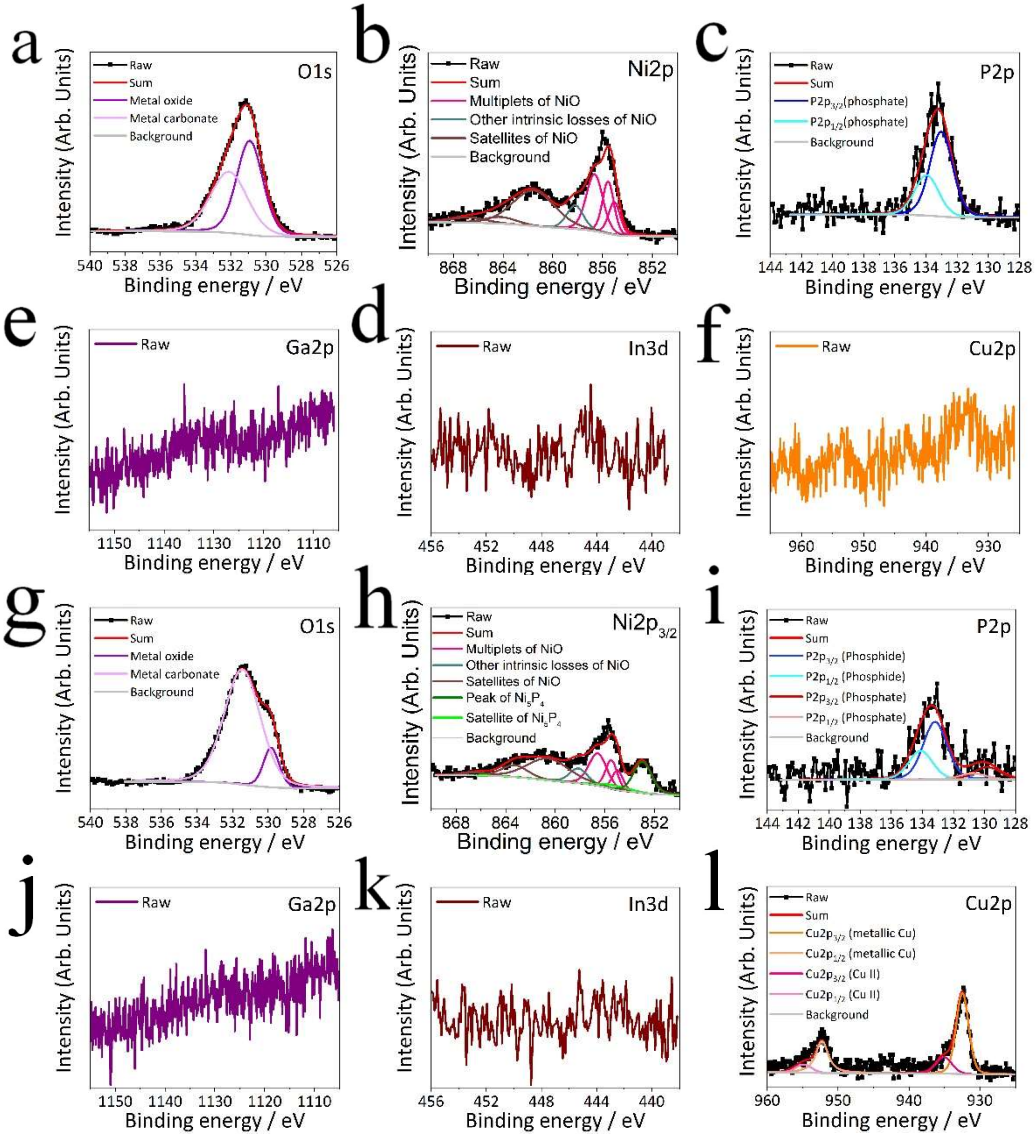

Figure S10 XPS post-analysis of the surfaces of the $Ni_5P_4/TiO_2/TiN/GaInP_2/GaAs$ III-V tandem photocathodes. a-f and **g-l**, XPS spectra including O1s, Ni2p, P2p, Ga2p, In3d and Cu2p spectra of the photocathode surfaces after the CA durability analysis for ~ 5 h and ~ 25 h (at and after the photocurrent current peak in **Figure 8a**), respectively.

XPS analysis of all expected elements and Cu was performed on the surfaces of the $Ni_5P_4/TiO_2/TiN$/III-V tandem photocathodes after continuous PEC operations at different times. At the time when the photocurrent density peak of the green CA curve in **Figure 8a** occurred, the photocathode surface was covered with nickel (II) oxides and phosphate species (**Figure S10a-c**). The Ni_5P_4 surface is likely to be partially oxidized during catalysis, resulting in formation of NiO and PO_x. The PO_x may also come from the residual sodium phosphate electrolyte after rinsing the electrode with Millipore water and drying in air. However, the XPS peaks of Ni and P of Ni_5P_4 were not detected. The absence of significant Ga2p and In3d peaks in **Figure S10e and d** indicates that the leakage and corrosion of $GaInP_2$ was not observed. In addition, Cu contamination was not found (**Figure S10f**). After the photocurrent density peak (after operation for ~25 h), oxides including NiO and PO_x still remained on the photocathode surface as expected (**Figure S10g-i**). By contrast, the Ni2p and P2p peaks originating from Ni_5P_4 appeared. Again, $GaInP_2$ was not corroded (**Figure S10j-k**). However, Cu contamination was detected suggested by the appearance of metallic Cu and CuO (**Figure S10l**). AFM imaging was also performed on the surfaces of the same samples. It reveals that at the photocurrent density peak, the photocathode surface was covered by foreign nanoparticles agglomerates (**Figure S4a and b**) and after the photocurrent peak, the majority agglomerates disappeared, resulting in the direct contact between Ni_5P_4 and electrolyte (**Figure S4c**). This surface evolution explains the aforementioned XPS results. The agglomerates were investigated by EDX spectrum and mapping analysis. Different sizes of agglomerates were enriched with carbon and oxygen (**Figure S5-7**), which are expected to originate from the epoxy used for encapsulation. It is likely that the fresh epoxy surface would photo-corroded and the disrupted polymers that are polarized can be deposited on the photocathode surface.

Our observation indicates that these deposited polymers are resistant to the pH7 electrolyte for a couple of hours under continuous PEC operation. By contrast, the epoxy coverage was not observed on the Ni_5P_4/TiN/n^+p$GaInP_2$ surface during photoelectrolysis in acid.[1] This is due to instability of epoxy in acid. The proposed physical degradation is that the ionic species of acids including hydroniums and anions can diffuse into epoxy and bind to the polar moieties, disrupting the noncovalent bonding within the polymer network.[2] This is not likely to happen to sodium phosphates that we used in this work due the larger sizes of their cations and polyatomic anions. That is why the epoxy coverage was observed initially. However, the deposited polymers cannot survive from the electrical field generated by the photovoltage and H_2 bubbling. The mechanisms behind photocorrosion of epoxy in different electrolytes are needed to be revealed in the future. The Cu contamination on the photocathode surface with further the durability test was confirmed by EDX spectroscopy analysis. (**Figure S8-9**). Cu contamination has been proved to cause slow degradation of photoelectrodes during long-term durability tests,[1] which is consistent with our case.

Table S2 OER FE measurement results

Electrode	Electrolyte	FE for volumetric sample	FE for TOF-MS purity analysis sample
IrO_2-coated carbon	0.5 M sodium phosphate	95.3%	95.9%

The oxygen samples evolved in 1 M NaOH measured FEs of 95.3% and 95.9% for the volumetric and purity analysis samples, respectively.

The time-of-flight mass spectrometer (TOF-MS) measurement and calibration yielded CO_2 and CO at 0.0198% and 0.0173% from the sample collected in 0.5 M sodium phosphate. This translates to an oxygen purity of 99.963%.

1 Hwang, S. *et al.* Highly efficient and durable III–V semiconductor-catalyst photocathodes via a transparent protection layer. *Sustainable energy & fuels* **4**, 1437-1442 (2020).

2 Lim, J. S. K., Gan, C. L. & Hu, X. M. Unraveling the mechanistic origins of epoxy degradation in acids. *ACS omega* **4**, 10799-10808 (2019).